

High-mass dijet cross sections in photoproduction at HERA

ZEUS Collaboration

Abstract

Dijet differential cross sections for the reaction $e^+p \rightarrow e^+ + \text{jet} + \text{jet} + X$ in the photoproduction regime have been measured with the ZEUS detector at HERA using an integrated luminosity of 42.7 pb^{-1} . The cross sections are given for photon-proton centre-of-mass energies in the range $134 < W < 277 \text{ GeV}$. The differential cross sections as a function of the dijet mass, M^{jj} , and of the dijet angular variables have been measured for $47 < M^{\text{jj}} < 160 \text{ GeV}$ and compared to next-to-leading-order QCD calculations. The dijet events in the region $75 < M^{\text{jj}} < 100 \text{ GeV}$ have been used to derive a 95% C.L. upper limit on the cross section for Z^0 photoproduction of $\sigma_{e^+p \rightarrow e^+Z^0X} < 5.9 \text{ pb}$. Upper limits on the photoproduction of new heavy resonances decaying into two jets are also presented for masses in the range between 60 GeV and 155 GeV.

The ZEUS Collaboration

S. Chekanov, M. Derrick, D. Krakauer, S. Magill, B. Musgrave, A. Pellegrino, J. Repond,
R. Yoshida

Argonne National Laboratory, Argonne, Illinois 60439-4815ⁿ

M.C.K. Mattingly

Andrews University, Berrien Springs, Michigan 49104-0380

P. Antonioli, G. Bari, M. Basile, L. Bellagamba, D. Boscherini, A. Bruni, G. Bruni,
G. Cara Romeo, L. Cifarelli, F. Cindolo, A. Contin, M. Corradi, S. De Pasquale, P. Giusti,
G. Iacobucci, G. Levi, A. Margotti, T. Massam, R. Nania, F. Palmonari, A. Pesci, G. Sar-
torelli, A. Zichichi

University and INFN Bologna, Bologna, Italy^e

G. Aghuzumtsyan, D. Bartsch, I. Brock, J. Crittenden¹, S. Goers, H. Hartmann, E. Hilger,
P. Irrgang, H.-P. Jakob, A. Kappes, U.F. Katz², R. Kerger, O. Kind, E. Paul, J. Rautenberg³,
R. Renner, H. Schnurbusch, A. Stifutkin, J. Tandler, K.C. Voss, A. Weber, H. Wessolek
Physikalisches Institut der Universität Bonn, Bonn, Germany^b

D.S. Bailey⁴, N.H. Brook⁴, J.E. Cole, B. Foster, G.P. Heath, H.F. Heath, S. Robins,
E. Rodrigues⁵, J. Scott, R.J. Tapper, M. Wing

H.H. Wills Physics Laboratory, University of Bristol, Bristol, United Kingdom^m

M. Capua, A. Mastroberardino, M. Schioppa, G. Susinno

Calabria University, Physics Department and INFN, Cosenza, Italy^e

H.Y. Jeoung, J.Y. Kim, J.H. Lee, I.T. Lim, K.J. Ma, M.Y. Pac⁶

Chonnam National University, Kwangju, Korea^g

A. Caldwell, M. Helbich, X. Liu, B. Mellado, S. Paganis, W.B. Schmidke, F. Sciulli

Nevis Laboratories, Columbia University, Irvington on Hudson, New York 10027^o

J. Chwastowski, A. Eskreys, J. Figiel, K. Olkiewicz, M.B. Przybycień⁷, P. Stopa, L. Za-
wiejski

Institute of Nuclear Physics, Cracow, Polandⁱ

B. Bednarek, I. Grabowska-Bold, K. Jeleń, D. Kisielewska, A.M. Kowal⁸, M. Kowal,
T. Kowalski, B. Mindur, M. Przybycień, E. Rulikowska-Zarębska, L. Suszycki, D. Szuba,
J. Szuba⁹

*Faculty of Physics and Nuclear Techniques, University of Mining and Metallurgy, Cracow,
Polandⁱ*

A. Kotański, W. Słomiński¹⁰

Department of Physics, Jagellonian University, Cracow, Poland

L.A.T. Bauerdick¹¹, U. Behrens, K. Borras, V. Chiochia, D. Dannheim, K. Desler¹², G. Drews, J. Fourletova, A. Fox-Murphy, U. Fricke, A. Geiser, F. Goebel, P. Göttlicher, R. Graciani, T. Haas, W. Hain, G.F. Hartner, S. Hillert, U. Kötz, H. Kowalski, H. Labes, D. Lelas, B. Löhr, R. Mankel, J. Martens¹³, M. Martínez¹¹, M. Moritz, D. Notz, M.C. Petrucci, A. Polini, U. Schneekloth, F. Selonke, S. Stonjek, B. Surrow¹⁴, J.J. Whitmore¹⁵, R. Wichmann¹⁶, G. Wolf, C. Youngman, W. Zeuner

Deutsches Elektronen-Synchrotron DESY, Hamburg, Germany

C. Coldewey¹⁷, A. Lopez-Duran Viani, A. Meyer, S. Schlenstedt

DESY Zeuthen, Zeuthen, Germany

G. Barbagli, E. Gallo, C. Genta, P. G. Pelfer

University and INFN, Florence, Italy^e

A. Bamberger, A. Benen, N. Coppola, P. Markun, H. Raach, S. Wölffe

Fakultät für Physik der Universität Freiburg i.Br., Freiburg i.Br., Germany^b

M. Bell, P.J. Bussey, A.T. Doyle, C. Glasman, S. Hanlon, S.W. Lee, A. Lupi, G.J. McCance, D.H. Saxon, I.O. Skillicorn

Department of Physics and Astronomy, University of Glasgow, Glasgow, United Kingdom^m

B. Bodmann, U. Holm, H. Salehi, K. Wick, A. Ziegler, Ar. Ziegler

Hamburg University, I. Institute of Exp. Physics, Hamburg, Germany^b

T. Carli, I. Gialas¹⁸, K. Klimek, E. Lohrmann, M. Milite

Hamburg University, II. Institute of Exp. Physics, Hamburg, Germany^b

C. Collins-Tooth, C. Foudas, R. Gonçalo⁵, K.R. Long, F. Metlica, D.B. Miller, A.D. Tapper, R. Walker

Imperial College London, High Energy Nuclear Physics Group, London, United Kingdom^m

P. Cloth, D. Filges

Forschungszentrum Jülich, Institut für Kernphysik, Jülich, Germany

M. Kuze, K. Nagano, K. Tokushuku¹⁹, S. Yamada, Y. Yamazaki

Institute of Particle and Nuclear Studies, KEK, Tsukuba, Japan^f

A.N. Barakbaev, E.G. Boos, N.S. Pokrovskiy, B.O. Zhautykov

Institute of Physics and Technology of Ministry of Education and Science of Kazakhstan, Almaty, Kazakhstan

S.H. Ahn, S.B. Lee, S.K. Park

Korea University, Seoul, Korea^g

H. Lim, D. Son

Kyungpook National University, Taegu, Korea^g

F. Barreiro, G. García, O. González, L. Labarga, J. del Peso, I. Redondo²⁰, J. Terrón,
M. Vázquez

Departamento de Física Teórica, Universidad Autónoma Madrid, Madrid, Spain^l

M. Barbi, A. Bertolin, F. Corriveau, A. Ochs, S. Padhi, D.G. Stairs, M. St-Laurent

Department of Physics, McGill University, Montréal, Québec, Canada H3A 2T8^a

T. Tsurugai

Meiji Gakuin University, Faculty of General Education, Yokohama, Japan

A. Antonov, V. Bashkirov²¹, P. Danilov, B.A. Dolgoshein, D. Gladkov, V. Sosnovtsev,
S. Suchkov

Moscow Engineering Physics Institute, Moscow, Russia^j

R.K. Dementiev, P.F. Ermolov, Yu.A. Golubkov, I.I. Katkov, L.A. Khein, N.A. Korotkova,
I.A. Korzhavina, V.A. Kuzmin, B.B. Levchenko, O.Yu. Lukina, A.S. Proskuryakov, L.M. Shche-
glova, A.N. Solomin, N.N. Vlasov, S.A. Zotkin

Moscow State University, Institute of Nuclear Physics, Moscow, Russia^k

C. Bokel, J. Engelen, S. Grijpink, E. Koffeman, P. Kooijman, E. Maddox, S. Schagen,
E. Tassi, H. Tiecke, N. Tuning, J.J. Velthuis, L. Wiggers, E. de Wolf

NIKHEF and University of Amsterdam, Amsterdam, Netherlands^h

N. Brümmner, B. Bylsma, L.S. Durkin, J. Gilmore, C.M. Ginsburg, C.L. Kim, T.Y. Ling

*Physics Department, Ohio State University, Columbus, Ohio 43210*ⁿ

S. Boogert, A.M. Cooper-Sarkar, R.C.E. Devenish, J. Ferrando, T. Matsushita, M. Rigby,
O. Ruske²², M.R. Sutton, R. Walczak

Department of Physics, University of Oxford, Oxford United Kingdom^m

R. Brugnera, R. Carlin, F. Dal Corso, S. Dusini, A. Garfagnini, S. Limentani, A. Longhin,
A. Parenti, M. Posocco, L. Stanco, M. Turcato

Dipartimento di Fisica dell' Università and INFN, Padova, Italy^e

L. Adamczyk²³, B.Y. Oh, P.R.B. Saull²³

*Department of Physics, Pennsylvania State University, University Park, Pennsylvania
16802*^o

Y. Iga

Polytechnic University, Sagamihara, Japan^f

G. D'Agostini, G. Marini, A. Nigro

Dipartimento di Fisica, Università 'La Sapienza' and INFN, Rome, Italy^e

C. Cormack, J.C. Hart, N.A. McCubbin
Rutherford Appleton Laboratory, Chilton, Didcot, Oxon, United Kingdom^m

C. Heusch
*University of California, Santa Cruz, California 95064*ⁿ

I.H. Park
Seoul National University, Seoul, Korea

N. Pavel
Fachbereich Physik der Universität-Gesamthochschule Siegen, Germany

H. Abramowicz, S. Dagan, A. Gabareen, S. Kananov, A. Kreisel, A. Levy
Raymond and Beverly Sackler Faculty of Exact Sciences, School of Physics, Tel-Aviv University, Tel-Aviv, Israel^d

T. Abe, T. Fusayasu, T. Kohno, K. Umemori, T. Yamashita
Department of Physics, University of Tokyo, Tokyo, Japan^f

R. Hamatsu, T. Hirose, M. Inuzuka, S. Kitamura²⁴, K. Matsuzawa, T. Nishimura
Tokyo Metropolitan University, Department of Physics, Tokyo, Japan^f

M. Arneodo²⁵, N. Cartiglia, R. Cirio, M. Costa, M.I. Ferrero, S. Maselli, V. Monaco, C. Peroni, M. Ruspa, R. Sacchi, A. Solano, A. Staiano
Università di Torino, Dipartimento di Fisica Sperimentale and INFN, Torino, Italy^e

R. Galea, T. Koop, G.M. Levman, J.F. Martin, A. Mirea, A. Sabetfakhri
Department of Physics, University of Toronto, Toronto, Ontario, Canada M5S 1A7^a

J.M. Butterworth, C. Gwenlan, R. Hall-Wilton, M.E. Hayes²⁶, E.A. Heaphy, T.W. Jones, J.B. Lane, M.S. Lightwood, B.J. West
Physics and Astronomy Department, University College London, London, United Kingdom^m

J. Ciborowski²⁷, R. Ciesielski, G. Grzelak, R.J. Nowak, J.M. Pawlak, B. Smalska²⁸, J. Sztuk²⁹, T. Tymieniecka³⁰, A. Ukleja³⁰, J. Ukleja, J.A. Zakrzewski, A.F. Żarnecki
*Warsaw University, Institute of Experimental Physics, Warsaw, Poland*ⁱ

M. Adamus, P. Plucinski
*Institute for Nuclear Studies, Warsaw, Poland*ⁱ

Y. Eisenberg, L.K. Gladilin³¹, D. Hochman, U. Karshon
Department of Particle Physics, Weizmann Institute, Rehovot, Israel^c

J. Breitweg³², D. Chapin, R. Cross, D. Kçira, S. Lammers, D.D. Reeder, A.A. Savin,
W.H. Smith

Department of Physics, University of Wisconsin, Madison, Wisconsin 53706ⁿ

A. Deshpande, S. Dhawan, V.W. Hughes, P.B. Straub

Department of Physics, Yale University, New Haven, Connecticut 06520-8121ⁿ

S. Bhadra, C.D. Catterall, S. Fourletov, S. Menary, M. Soares, J. Standage

Department of Physics, York University, Ontario, Canada M3J 1P3^a

- ¹ now at Cornell University, Ithaca/NY, USA
- ² on leave of absence at University of Erlangen-Nürnberg, Germany
- ³ supported by the GIF, contract I-523-13.7/97
- ⁴ PPARC Advanced fellow
- ⁵ supported by the Portuguese Foundation for Science and Technology (FCT)
- ⁶ now at Dongshin University, Naju, Korea
- ⁷ now at Northwestern Univ., Evanston/IL, USA
- ⁸ supported by the Polish State Committee for Scientific Research, grant no. 5 P-03B 13720
- ⁹ partly supported by the Israel Science Foundation and the Israel Ministry of Science
- ¹⁰ Department of Computer Science, Jagellonian University, Cracow
- ¹¹ now at Fermilab, Batavia/IL, USA
- ¹² now at DESY group MPY
- ¹³ now at Philips Semiconductors Hamburg, Germany
- ¹⁴ now at Brookhaven National Lab., Upton/NY, USA
- ¹⁵ on leave from Penn State University, USA
- ¹⁶ now at Mobilcom AG, Rendsburg-Büdelndorf, Germany
- ¹⁷ now at GFN Training GmbH, Hamburg
- ¹⁸ Univ. of the Aegean, Greece
- ¹⁹ also at University of Tokyo
- ²⁰ supported by the Comunidad Autonoma de Madrid
- ²¹ now at Loma Linda University, Loma Linda, CA, USA
- ²² now at IBM Global Services, Frankfurt/Main, Germany
- ²³ partly supported by Tel Aviv University
- ²⁴ present address: Tokyo Metropolitan University of Health Sciences, Tokyo 116-8551, Japan
- ²⁵ also at Università del Piemonte Orientale, Novara, Italy
- ²⁶ now at CERN, Geneva, Switzerland
- ²⁷ also at Łódź University, Poland
- ²⁸ supported by the Polish State Committee for Scientific Research, grant no. 2 P-03B 00219
- ²⁹ Łódź University, Poland
- ³⁰ sup. by Pol. State Com. for Scien. Res., 5 P-03B 09820 and by Germ. Fed. Min. for Edu. and Research (BMBF), POL 01/043
- ³¹ on leave from MSU, partly supported by University of Wisconsin via the U.S.-Israel BSF
- ³² now at EssNet Deutschland GmbH, Hamburg, Germany

- a* supported by the Natural Sciences and Engineering Research Council of Canada (NSERC)
- b* supported by the German Federal Ministry for Education and Research (BMBF), under contract numbers HZ1GUA 2, HZ1GUB 0, HZ1PDA 5, HZ1VFA 5
- c* supported by the MINERVA Gesellschaft für Forschung GmbH, the Israel Science Foundation, the U.S.-Israel Binational Science Foundation, the Israel Ministry of Science and the Benozvio Center for High Energy Physics
- d* supported by the German-Israeli Foundation, the Israel Science Foundation, and by the Israel Ministry of Science
- e* supported by the Italian National Institute for Nuclear Physics (INFN)
- f* supported by the Japanese Ministry of Education, Science and Culture (the Monbusho) and its grants for Scientific Research
- g* supported by the Korean Ministry of Education and Korea Science and Engineering Foundation
- h* supported by the Netherlands Foundation for Research on Matter (FOM)
- i* supported by the Polish State Committee for Scientific Research, grant no. 115/E-343/SPUB-M/DESY/P-03/DZ 121/2001-2002
- j* partially supported by the German Federal Ministry for Education and Research (BMBF)
- k* supported by the Fund for Fundamental Research of Russian Ministry for Science and Education and by the German Federal Ministry for Education and Research (BMBF)
- l* supported by the Spanish Ministry of Education and Science through funds provided by CICYT
- m* supported by the Particle Physics and Astronomy Research Council, UK
- n* supported by the US Department of Energy
- o* supported by the US National Science Foundation

1 Introduction

In hadronic interactions, the distributions of the dijet mass, M^{jj} , and of the angle, θ^{CM} , between the jet-jet axis and the beam direction in the dijet centre-of-mass system, provide a test of QCD. In addition, they are sensitive to the presence of new particles that decay into two jets. At HERA, these tests of QCD and searches for new particles can be made in photoproduction via ep scattering at $Q^2 \approx 0$, where Q^2 is the virtuality of the exchanged photon. Two types of QCD processes contribute to jet production at leading order (LO) in photoproduction [1, 2]: either the photon interacts directly with a parton in the proton (the direct process) or the photon acts as a source of partons, one of which interacts with a parton in the proton (the resolved process). Jet photoproduction thereby provides a means to study the dynamics of both photon-parton and parton-parton interactions.

At high M^{jj} values, the theoretical uncertainties due to hadronisation, multipartonic interactions and the limited knowledge of the photon parton densities are reduced. The dynamics of dijet production for hadron-induced processes has been investigated in detail in $p\bar{p}$ collisions at centre-of-mass energies of $\sqrt{s} = 630$ GeV [3, 4] and $\sqrt{s} = 1800$ GeV [5]. Next-to-leading-order (NLO) QCD predictions are in good agreement with the measured dijet mass and angular distributions up to $M^{\text{jj}} \approx 1000$ GeV. Previous measurements of the dijet mass and angular distributions [3–6] made use of cone algorithms for the identification of the jets. The k_T cluster algorithm [7, 8] is used here, which allows a direct application of the theoretical jet algorithm to the data. The selection of high M^{jj} values permits a precise test of the description of the dynamics of dijet photoproduction to smaller distances than previously studied in photoproduction at HERA [6].

Heavy particles that decay into two jets would show up as an enhancement in the dijet mass distribution. In particular, this mass distribution is sensitive to the production of the electroweak gauge bosons W^\pm and Z^0 . New heavy particles decaying into two jets may also be identified by deviations from the predictions of QCD in the $|\cos\theta^{\text{CM}}|$ distribution; in QCD, the $|\cos\theta^{\text{CM}}|$ distribution is peaked at unity, whereas many sources of new physics produce more isotropic angular distributions.

In this paper, measurements of the dijet differential cross-sections $d\sigma/dM^{\text{jj}}$ and $1/\sigma d\sigma/d\chi$, where $\chi \equiv (1 + |\cos\theta^*|)/(1 - |\cos\theta^*|)$, are presented as a function of M^{jj} . The variable θ^* is defined by using the pseudorapidities¹ of the two jets with highest transverse energy in the event, $\cos\theta^* \equiv \tanh\frac{1}{2}(\eta^{\text{jet1}} - \eta^{\text{jet2}})$, and coincides with θ^{CM} for the case of $2 \rightarrow 2$ massless parton scattering. To increase the sensitivity to direct processes, measurements have also been made for dijet events in which the fraction of the photon's momentum participating in the production of the dijet system is greater than 0.75. The NLO QCD

¹ The pseudorapidity is defined as $\eta = -\ln(\tan\frac{\theta}{2})$, where the polar angle, θ , is measured with respect to the proton beam direction.

calculations [9–12] are compared to the present measurements and upper limits are set on the inclusive cross sections for the photoproduction of W^\pm and Z^0 bosons. A search has also been carried out for the photoproduction of new heavy resonances decaying into two jets.

2 Perturbative QCD calculations

Perturbative QCD (pQCD) calculations of dijet cross sections in photoproduction can be written as a convolution of the subprocess cross section with the parton distribution functions (PDFs) of the photon and proton:

$$d\sigma_{ep \rightarrow e \text{ jet jet} X} = \sum_{a,b} \int_0^1 dy f_{\gamma/e}(y) \int_0^1 dx_\gamma f_{a/\gamma}(x_\gamma, \mu_{F\gamma}^2) \int_0^1 dx_p f_{b/p}(x_p, \mu_{Fp}^2) d\hat{\sigma}_{ab \rightarrow \text{jet jet}}(\mu_R),$$

where y , x_γ and x_p are the longitudinal momentum fractions of the quasi-real photon emitted by the positron, the parton a in the photon and the parton b in the proton, respectively; $f_{\gamma/e}$ is the flux of photons in the positron and is usually estimated with the Weizsäcker-Williams approximation [13]; $f_{a/\gamma}$ ($f_{b/p}$) represents the PDF of parton a (b) in the photon (proton) – in the case of direct processes, a is a γ and $f_{a/\gamma}(x_\gamma, \mu_{F\gamma}^2)$ is given by $\delta(1 - x_\gamma)$; the factorisation scale in the photon (proton) is denoted by $\mu_{F\gamma}$ (μ_{Fp}); μ_R represents the renormalisation scale; and the subprocess cross section, $d\hat{\sigma}_{ab \rightarrow \text{jet jet}}$, describes the short-distance structure of the interaction.

A wealth of data from fixed-target and collider experiments has made possible an accurate determination of the proton PDFs. In the case of the photon, experimental information on the quark densities is available from measurements of F_2^γ in e^+e^- collisions, while the gluon density remains poorly constrained. At high values of the dijet mass, the direct processes dominate and thus the sensitivity to the photon PDFs is reduced.

The subprocess cross section is calculable in pQCD at each order. Recently, NLO QCD calculations in photoproduction [9–12] have become available. In NLO QCD, the dependence of the calculations on the renormalisation and factorisation scales is reduced compared to LO. The results from the different NLO calculations have been compared and found to be in agreement within 5% in most of the phase-space region studied [14].

3 Experimental conditions

During 1995-1997, HERA operated with protons of energy $E_p = 820$ GeV and positrons of energy $E_e = 27.5$ GeV. The data sample used in this analysis corresponds to an integrated luminosity of 42.7 ± 0.7 pb $^{-1}$. The ZEUS detector is described in detail elsewhere [15, 16].

The main subdetectors used in the present analysis are the central tracking detector (CTD) positioned in a 1.43 T solenoidal magnetic field and the uranium-scintillator sampling calorimeter (CAL).

Tracking information is provided by the CTD [17], which is used to reconstruct the momenta of tracks in the polar-angle² region $15^\circ < \theta < 164^\circ$. The relative transverse momentum, p_T , resolution for full-length tracks can be parameterised as $\sigma(p_T)/p_T = 0.0058 p_T \oplus 0.0065 \oplus 0.0014/p_T$, with p_T in GeV. The tracking system was used to establish an interaction vertex with a typical resolution along (transverse to) the beam direction of 0.4 (0.1) cm and to cross-check the energy scale of the CAL.

The CAL [18] covers 99.7% of the total solid angle. The smallest subdivision of the CAL is called a cell. Energy deposits in the CAL were used in the jet finding and to measure jet energies. Under test-beam conditions, the CAL single-particle relative energy resolutions were $0.18/\sqrt{E(\text{GeV})}$ for electrons and $0.35/\sqrt{E(\text{GeV})}$ for hadrons. Jet energies were corrected (see Section 6) for the energy lost in inactive material in front of the CAL.

The luminosity was measured using the Bethe-Heitler reaction $e^+p \rightarrow e^+\gamma p$ [19]. The resulting small-angle energetic photons were measured by the luminosity monitor, a lead-scintillator calorimeter placed in the HERA tunnel at $Z = -107$ m.

4 Data selection and jet search

A three-level trigger was used to select events online [16, 20]. Events from collisions between quasi-real photons and protons were selected offline using criteria similar to those described in an earlier ZEUS publication [21]. The main steps are briefly discussed here. After requiring a reconstructed event vertex consistent with the nominal interaction position and cuts based on the tracking information, the contamination from beam-gas interactions, cosmic-ray showers and beam-halo muons was negligible. Charged current deep inelastic scattering (DIS) events were rejected by requiring the total missing transverse momentum, \cancel{p}_T , to be small compared to the total transverse energy, E_T^{tot} : $\cancel{p}_T/\sqrt{E_T^{\text{tot}}} < 2\sqrt{\text{GeV}}$. Neutral current DIS events with an identified scattered-positron candidate [22] in the CAL were removed from the sample using the method described in an earlier publication [23]. The remaining background from neutral current DIS events was estimated by Monte Carlo techniques to be below 0.5%. The selected sample consisted of events from e^+p interactions with $Q^2 \lesssim 1 \text{ GeV}^2$ and a median $Q^2 \approx 10^{-3} \text{ GeV}^2$. The events were restricted to γp centre-of-mass energies in the range $134 < W < 277 \text{ GeV}$, as described in Section 7.

² The ZEUS coordinate system is a right-handed Cartesian system, with the Z axis pointing in the proton beam direction, referred to as the “forward direction”, and the X axis pointing left towards the centre of HERA. The coordinate origin is at the nominal interaction point.

The k_T cluster algorithm [7] was used in the longitudinally invariant inclusive mode [24] to reconstruct jets in the hadronic final state from the energy deposits in the CAL cells. The jet search was performed in the pseudorapidity (η)-azimuth (φ) plane of the laboratory frame. The jet variables were defined according to the Snowmass convention [25]. The jets reconstructed from the CAL cell energies are called calorimetric jets and the variables associated with them are denoted by $E_{T,\text{cal}}^{\text{jet}}$, $\eta_{\text{cal}}^{\text{jet}}$ and $\varphi_{\text{cal}}^{\text{jet}}$. There were 64708 events selected with at least two jets satisfying $E_{T,\text{cal}}^{\text{jet}} > 10$ GeV and $-1 < \eta_{\text{cal}}^{\text{jet}} < 2.5$.

5 Monte Carlo simulation

The Monte Carlo (MC) programs PYTHIA 5.7 [26] and HERWIG 5.9 [27] were used to generate photoproduction events for resolved and direct processes. Events were generated using GRV-HO [28] for the photon PDFs and MRSA [29] for the proton PDFs. To study the dependence of the acceptance corrections on the choice of photon PDFs, the LAC1 parameterisations [30] were used. In both generators, the partonic processes are simulated using LO matrix elements, with the inclusion of initial- and final-state parton showers. Fragmentation into hadrons is performed using the LUND [31] string model as implemented in JETSET [32] in the case of PYTHIA, and the cluster model [33] in the case of HERWIG. For the measurements presented in this paper, the events generated using the PYTHIA and HERWIG programs were used for calculating jet-energy corrections and correcting for detector and acceptance effects. The corrections provided by PYTHIA were used as default values and those given by HERWIG were used to estimate the systematic uncertainties coming from the treatment of the parton shower and hadronisation.

Photoproduction of the electroweak gauge bosons W^\pm and Z^0 was simulated with PYTHIA using the lowest-order processes $q\bar{q} \rightarrow Z^0$ and $q\bar{q}' \rightarrow W^\pm$. Events were generated, including initial- and final-state parton showers, using GRV-HO for the photon and MRSA for the proton PDFs.

To model the photoproduction of narrow heavy resonances decaying to dijets, MC events were simulated with PYTHIA using the LO process $q\bar{q} \rightarrow Z'$ and the same photon and proton PDFs as above. Samples of events were generated for each value of the mass from 60 GeV up to 155 GeV in 5 GeV intervals. The vector and axial couplings to quarks and leptons were set equal to those of the Standard Model Z^0 , resulting in a width that increases linearly with mass. The cut $|\cos\theta^*| < 0.6$ was used to minimise the sensitivity of the acceptance corrections to the *a priori* unknown decay angular distribution of a new narrow state.

All generated events were passed through the ZEUS detector and trigger simulation programs based on GEANT 3.13 [34]. They were reconstructed and analysed by the same program chain as the data. The jet search was performed using the energy measured in

the CAL cells in the same way as for the data. The same jet algorithm was also applied to the final-state particles; the jets found in this way are referred to as hadronic jets.

6 Jet energy correction and selection

6.1 Jet hadron-level corrections

The comparison of the reconstructed jet variables for the hadronic and the calorimetric jets in simulated events showed that no correction was needed for η^{jet} and φ^{jet} ($\eta^{\text{jet}} \simeq \eta_{\text{cal}}^{\text{jet}}$ and $\varphi^{\text{jet}} \simeq \varphi_{\text{cal}}^{\text{jet}}$). However, the transverse energy of the calorimetric jet underestimated that of the corresponding hadronic jet by an average of $\sim 15\%$, with an r.m.s. of $\sim 10\%$. The transverse energy corrections to calorimetric jets, averaged over the azimuthal angle, were first determined using the MC events. These corrections were constructed as factors, $C(E_{T,\text{cal}}^{\text{jet}}, \eta_{\text{cal}}^{\text{jet}})$, which, when multiplied by $E_{T,\text{cal}}^{\text{jet}}$, provide the corrected transverse energies of the jets, E_T^{jet} .

6.2 Jet energy-scale corrections

Further corrections to the jet transverse energy were developed to account for differences in the jet energy scale between data and simulations. This procedure relies on good understanding of the performance of the CTD track reconstruction in the selected region (see below).

The response of the CAL to jets was investigated by using the following procedure [21, 35]. In the central region, $|\eta^{\text{jet}}| < 1$, the multiplicity distribution and the p_T spectrum of charged particles associated with the calorimetric jets were compared for data and MC samples using the reconstructed tracks. The tracks were required to be in the ranges $|\eta^{\text{track}}| < 1.5$ and $p_T^{\text{track}} > 300$ MeV, where p_T^{track} is the transverse momentum of the track with respect to the beam axis and η^{track} is the track pseudorapidity. Tracks were associated with a calorimetric jet when the extrapolated track trajectory reached the CAL within a cone of one unit radius in the η - φ plane concentric with the calorimetric-jet axis. PYTHIA gives a good description of all the measured distributions. In this η^{jet} region, the momenta of the tracks in the calorimetric jet were used to determine the total transverse energy carried by the charged particles, $E_{T,\text{tracks}}^{\text{jet}}$, assuming zero mass for all tracks. Then, the ratio $r_{\text{tracks}} \equiv E_{T,\text{tracks}}^{\text{jet}}/E_{T,\text{cal}}^{\text{jet}}$ was calculated and the distributions of this ratio for the dijet sample in data and MC generated events were compared. The mean value of the distribution in r_{tracks} was determined as a function of η^{jet} for data ($\langle r_{\text{tracks}} \rangle_{\text{data}}$) and MC events ($\langle r_{\text{tracks}} \rangle_{\text{MC}}$). Differences between data and MC simulation of less than 1% were observed from the examination of the quantity $(\langle r_{\text{tracks}} \rangle_{\text{data}} / \langle r_{\text{tracks}} \rangle_{\text{MC}}) - 1$. The

transverse energies of the calorimetric jets in the data were then modified as a function of η^{jet} to correct for these differences.

In the forward region, $1 < \eta^{\text{jet}} < 2.5$, the energy scale of the jets was studied using the transverse-energy imbalance in dijet events with one jet in the central region and the other in the forward region. The distributions of the ratio $r_{\text{dijet}} \equiv E_{T,\text{cal}}^{\text{jet}}(\text{forward jet})/E_{T,\text{cal}}^{\text{jet}}(\text{central jet})$ in data and the MC sample were compared. Differences between data and MC simulation of less than 2% were observed from the examination of the quantity $(\langle r_{\text{dijet}} \rangle_{\text{data}} / \langle r_{\text{dijet}} \rangle_{\text{MC}}) - 1$. The transverse energies of the forward calorimetric jets in the data were then modified as a function of η^{jet} to correct for these differences. The widths of the distributions for r_{tracks} and r_{dijet} are reasonably well described by the PYTHIA MC simulation, giving confidence that the resolution in the energy of the jets is correctly described.

The accuracy of the jet energy corrections was investigated by using data and simulations of neutral current DIS events at large Q^2 , where the transverse energy of the jet or jets is balanced by that of the scattered positron. The uncertainty in the absolute CAL energy calibration for the scattered positrons was 1% for positron energies above 15 GeV [36]. Jets were reconstructed in the laboratory frame using the algorithm described in Section 4. The jet energy corrections described above were applied to both data and MC events. Then, the ratio $r_{e/\text{jet}} \equiv E_T^e/E_T^{\text{jet}}$, where E_T^e is the positron transverse energy, was formed and the distributions of this ratio for the inclusive jet sample in DIS data and MC simulation were compared. The mean value of the distribution of $r_{e/\text{jet}}$ was determined as a function of η^{jet} in the range $-1 < \eta^{\text{jet}} < 2.5$ and of E_T^{jet} in the range $14 < E_T^{\text{jet}} < 90$ GeV for data ($\langle r_{e/\text{jet}} \rangle_{\text{data}}$) and MC events ($\langle r_{e/\text{jet}} \rangle_{\text{MC}}$). Inspection of the quantity $|\langle r_{e/\text{jet}} \rangle_{\text{data}} / \langle r_{e/\text{jet}} \rangle_{\text{MC}} - 1|$ showed that the differences between data and MC simulation were smaller than 1%. This variation was therefore included as a systematic uncertainty in the present analysis.

After these further corrections to the jet transverse energy, events with at least two jets satisfying $E_T^{\text{jet}} > 14$ GeV and $-1 < \eta^{\text{jet}} < 2.5$ were used to measure the dijet cross sections presented in Section 9.

7 Reconstruction of jet and kinematic variables

The invariant mass of the two jets with highest E_T^{jet} in the event was reconstructed using the formula

$$M^{\text{jj}} = \sqrt{2E_T^{\text{jet1}}E_T^{\text{jet2}}[\cosh(\eta^{\text{jet1}} - \eta^{\text{jet2}}) - \cos(\varphi^{\text{jet1}} - \varphi^{\text{jet2}})]}.$$

Only the absolute value of $\cos\theta^*$ can be determined because the originating parton cannot be identified. For $M^{\text{jj}} > 47$ GeV and $|\cos\theta^*| < 0.8$, the average relative resolutions in

M^{jj} and χ were 8% and 7%, respectively; the average resolution in $|\cos\theta^*|$ was 0.02.

The Jacquet-Blondel method [37], applied to photoproduction events [38], was used to estimate W from the energies measured in the CAL cells, W_{cal} . Due to the energy lost in the inactive material in front of the CAL and to particles lost in the rear beampipe, W_{cal} underestimates W by $\sim 10\%$, with an r.m.s. of $\sim 5\%$ [20]. This effect was corrected for using the MC simulation.

The fraction of the photon momentum participating in the production of the two jets with highest E_T^{jet} is defined [23, 39] as

$$x_\gamma^{\text{obs}} = \frac{1}{2yE_e} (E_T^{\text{jet1}} e^{-\eta^{\text{jet1}}} + E_T^{\text{jet2}} e^{-\eta^{\text{jet2}}}), \quad (1)$$

where the variable y is given by $y = W^2/s$. The LO direct and resolved processes populate different regions in x_γ^{obs} , with the direct processes concentrated at high values of x_γ^{obs} . The variable x_γ^{obs} was reconstructed via the above formula using the calorimetric-jet transverse energies and $y_{\text{cal}} = W_{\text{cal}}^2/s$, since many systematic uncertainties in the measurement of energy by the CAL cancel out event by event in the ratio of Eq. (1). The average resolution in x_γ^{obs} was 0.05 for $M^{\text{jj}} > 47$ GeV and $|\cos\theta^*| < 0.8$.

8 Acceptance corrections and systematic uncertainties

The PYTHIA MC event samples of resolved and direct processes were used to compute the acceptance corrections to the dijet distributions. These correction factors also take into account the efficiency of the trigger, the selection criteria and the purity and efficiency of the jet reconstruction. The contributions from direct and resolved processes in the MC models were added according to a fit to the uncorrected x_γ^{obs} distribution in the data. A good description of the M^{jj} , $|\cos\theta^*|$ and χ data distributions was given both by PYTHIA and HERWIG. The differential dijet cross sections were obtained by applying bin-by-bin corrections to the measured distributions. The bin-by-bin correction factors differed from unity typically by less than 10%.

A detailed study of the sources of systematic uncertainty was performed. This study includes (a typical contribution for each item to the cross-section uncertainty is indicated in parentheses):

- using the HERWIG generator to evaluate the correction factors for the observed dijet distributions (5%);
- varying the cuts used to select the data while maintaining agreement between data and MC simulations (2%);

- adding the contributions from direct and resolved processes according to the default cross sections as predicted by PYTHIA (2%);
- using the LAC1 parameterisations of the photon PDFs for the PYTHIA MC samples (2%).

The effects of uncertainties in the simulation of the trigger were negligible. All the above systematic uncertainties were added in quadrature to the statistical uncertainties.

The absolute energy scale of the calorimetric jets in simulated events was varied by $\pm 1\%$. The effect of this variation on the dijet cross sections was approximately $\mp 5\%$. This uncertainty is highly correlated between measurements in different bins. It is shown as a shaded band in Fig. 1. In Figs. 2 to 4, it has been added in quadrature to the other systematic uncertainties. An overall normalisation uncertainty of 1.6%, arising from the luminosity determination, is not included.

9 High-mass dijet differential cross sections

Using the selected data sample of dijet events, the differential dijet cross sections were measured in the kinematic region defined by $Q^2 \leq 1 \text{ GeV}^2$ and $134 < W < 277 \text{ GeV}$. The dijet variables and cross sections were calculated using the two highest- $E_T^{\text{j}et}$ hadronic jets with $E_T^{\text{j}et} > 14 \text{ GeV}$ and $-1 < \eta^{\text{j}et} < 2.5$. For a given W , events at high $|\cos\theta^*|$ have smaller scattering angles and thus lower $E_T^{\text{j}et}$. In order to study the $|\cos\theta^*|$ and $M^{\text{j}j}$ distributions without bias from the $E_T^{\text{j}et}$ requirement, the cuts $M^{\text{j}j} > 47 \text{ GeV}$ and $|\cos\theta^*| < 0.8$ were applied³.

The cross-section $d\sigma/dM^{\text{j}j}$, measured in the $M^{\text{j}j}$ range between 47 and 160 GeV and integrated over $|\cos\theta^*| < 0.8$, is presented in Fig. 1(a). The data points are located at the mean of each $M^{\text{j}j}$ bin. The measured $d\sigma/dM^{\text{j}j}$ exhibits a steep fall-off over 3 orders of magnitude in the $M^{\text{j}j}$ range considered.

The cross-section $d\sigma/dM^{\text{j}j}$ was also measured for the region $x_\gamma^{\text{obs}} > 0.75$. The results are also presented in Fig. 1(a) and exhibit a dependence on $M^{\text{j}j}$ similar to that of the measurements integrated over the full range in x_γ^{obs} . The fraction of dijet events with $x_\gamma^{\text{obs}} > 0.75$ increases with $M^{\text{j}j}$ from 57% at $M^{\text{j}j} = 50 \text{ GeV}$ to 98% at $M^{\text{j}j} = 139 \text{ GeV}$.

To study the angular distribution as a function of the dijet mass, the normalised dijet cross section, $1/\sigma d\sigma/d\chi$, was measured for $1 \leq \chi \leq 9$ in four regions of $M^{\text{j}j}$; σ is the

³ The application of a lower cut on $M^{\text{j}j}$ which is not close to the threshold avoids the infrared sensitivity [11] that otherwise would affect NLO QCD calculations for dijet production with symmetric cuts in the transverse energy of each of the two jets.

dijet cross section integrated over the entire χ range in each M^{jj} region. The normalised cross section has the advantage that the experimental and theoretical uncertainties are reduced, while allowing a precise test of the shape of the distribution in the calculations. The results integrated over the full range in x_γ^{obs} are presented in Fig. 2 and those in the region $x_\gamma^{\text{obs}} > 0.75$ are shown in Fig. 3. The measured $1/\sigma d\sigma/d\chi$ decreases with increasing χ in all the M^{jj} regions studied.

9.1 Perturbative QCD predictions

LO and NLO QCD calculations [9] are compared to the measurements in Figs. 1 to 3. The calculations were performed using the GRV [28] and CTEQ4 [40] parameterisations of the photon and proton PDFs, respectively. The renormalisation and factorisation scales were chosen to be the highest E_T^{jet} ; α_s was calculated at the two-loop level using $\Lambda_{\overline{\text{MS}}}^{(5)} = 202$ MeV, which corresponds to $\alpha_s(M_Z) = 0.116$. The calculations included only QCD hard-scattering processes and thus electroweak corrections such as $q\bar{q} \rightarrow q\bar{q}$ via γ^*/Z^0 exchange or $q\bar{q}' \rightarrow q\bar{q}'$ via W^\pm exchange were not included.

The uncertainty on the NLO calculations due to the absence of higher-order terms was estimated by varying the choice of the renormalisation and factorisation scales between $E_T^{\text{jet}}/2$ and $2E_T^{\text{jet}}$ and amounts to less than 15% in the case of $d\sigma/dM^{\text{jj}}$. This uncertainty affects mainly the normalisation of the predictions and is therefore reduced for $1/\sigma d\sigma/d\chi$, for which it typically amounts to less than 5%. The uncertainty on the NLO calculations due to that on the gluon density of the proton was estimated by comparing with calculations based on the CTEQ4HJ [40] parameterisations and amounts to less than 6% for $d\sigma/dM^{\text{jj}}$. The uncertainty due to the choice of photon PDFs was estimated by using the AFG [41] parameterisations. The choice of parameterisation of the photon PDFs affects mainly the normalisation of the calculation. The normalisation for the case of AFG is smaller by approximately 10% than that based on GRV. All the above theoretical uncertainties were added in quadrature.

NLO QCD calculations refer to jets of partons, whereas the measurements refer to jets of hadrons. An estimate of the effects of hadronisation was obtained by comparing the cross sections for jets of hadrons and jets of partons calculated with the PYTHIA program. The corrections for hadronisation effects were found to be within $\pm 5\%$ of unity both for $d\sigma/dM^{\text{jj}}$ and $1/\sigma d\sigma/d\chi$; they therefore were neglected in the comparison of pQCD calculations to the measurements.

9.2 Dijet mass distribution

The LO and NLO QCD calculations describe the shape of the measured $d\sigma/dM^{\text{jj}}$ well over the entire range of M^{jj} and x_γ^{obs} , see Fig. 1(a). The shape of this distribution in

the calculations is dictated by the x dependence of the photon and proton PDFs and by the dependence on the photon-parton or parton-parton centre-of-mass energy of the subprocess cross section. The LO QCD calculation of $d\sigma/dM^{\text{jj}}$ is $\sim 25\%$ below the data. The inclusion of the NLO corrections significantly improves the description of the data. Although the data are still consistently above the calculations, the NLO QCD calculations are consistent with the data given the present theoretical ($\sim 15\%$) and experimental ($\sim 10\%$) uncertainties, as shown in Fig. 1(b).

Since the region $x_\gamma^{\text{obs}} > 0.75$ is dominated by direct processes, in which the photon behaves as a point-like particle, measurements restricted to that region in x_γ^{obs} allow a test of the pQCD predictions with less influence from the photon PDFs. The NLO QCD predictions of $d\sigma/dM^{\text{jj}}$ have been compared to the data in the region $x_\gamma^{\text{obs}} > 0.75$. In this restricted range, the NLO QCD calculations describe the data well both in shape and magnitude, as shown in Fig. 1(c).

Overall, no significant deviation between data and NLO QCD calculations is observed up to $M^{\text{jj}} = 139$ GeV.

9.3 Dijet angular distribution

Figure 2 shows that the shape of the NLO QCD calculation is in agreement with that of the measured $1/\sigma d\sigma/d\chi$ in each region of dijet mass studied. An equally good description is obtained for the measurements restricted to $x_\gamma^{\text{obs}} > 0.75$, as can be seen in Fig. 3. The distribution in χ reflects the spin of the exchanged particle: it is approximately uniform for two-body processes dominated by gluon exchange [42] and proportional to $1/(1+\chi)$ for processes mediated by quark exchange. As an illustration, the LO QCD calculations for resolved and direct processes are shown in Fig. 2: the χ distribution for direct processes, which are mediated by quark exchange, is steeper than that of resolved processes, which are dominated by gluon exchange. The measured angular distribution is consistent with the pQCD description in terms of parton exchange up to the highest M^{jj} .

The ratio $R_\chi \equiv \frac{\sigma(1 < \chi < \chi_0)}{\sigma(\chi_0 < \chi < 9)}$ is useful to characterise, with a single number, the shape of the angular distribution in each range of dijet mass [4]. This ratio is shown in Fig. 4, with the value of χ_0 chosen to be 4, so that R_χ is approximately 1. In this ratio, most of the systematic uncertainties cancel out, yielding a systematic uncertainty of less than 4% for all M^{jj} ranges considered. The uncertainties of the theoretical predictions for R_χ due to the choice of photon PDFs and from the choice of renormalisation and factorisation scales are also reduced. The NLO QCD calculations are consistently below, but compatible with, the data within the experimental ($\sim 8\%$) and theoretical ($\sim 10\%$) uncertainties.

9.4 Upper limits on Z^0 , W^\pm and new heavy-resonance production

The production of the electroweak gauge bosons W^\pm and Z^0 has been studied in the region $75 < M^{\text{jj}} < 100$ GeV for the full range⁴ in x_γ^{obs} . The $1/\sigma d\sigma/d\chi$ distribution is not consistent with a large contribution from W^\pm and Z^0 decays, as can be seen from Fig. 2, which shows that QCD processes are dominant. Simulations of both the QCD (non-resonant) dijet photoproduction background and the Z^0 signal were used to find values that optimise the observation of a Z^0 signal relative to the background for the upper cut on the measured value of $|\cos\theta^*|$, $|\cos\theta^*|_{\text{cut}}$, and the dijet-mass window. The background expected from QCD processes was estimated by using the NLO QCD predictions with the normalisation obtained from a fit to the measured $d\sigma/dM^{\text{jj}}$ in the region $47 < M^{\text{jj}} < 75$ GeV. Since there is no evidence for a signal, an upper limit on the cross section for Z^0 production has been derived. In the dijet-mass window of 91 ± 9 GeV and for $|\cos\theta^*| < 0.6$, 230 events were observed while 223 events were expected from QCD processes. The acceptance for Z^0 production after all the selection cuts was 14.6%. The resulting 95% C.L. upper limit in the kinematic region $Q^2 \leq 1$ GeV² is

$$\sigma_{e^+p \rightarrow e^+Z^0X} < 5.9 \text{ pb.}$$

In deriving the upper limit, the two different photon PDFs mentioned in Section 9.1 were used; the one that gave the most conservative limit was chosen. This upper limit on Z^0 production is the first obtained at HERA. The Standard Model expectation for the process $e^+p \rightarrow e^+Z^0X$ integrated over all Q^2 is 0.3 pb [43,44]. The same procedure was applied for W^\pm production and an upper limit of $\sigma_{e^+p \rightarrow e^+W^\pm X} < 7.4$ pb at 95% C.L. was obtained. This limit is weaker than that already obtained by ZEUS using the W^\pm leptonic decays [44]. The Standard Model expectation for the cross section of the process $e^+p \rightarrow e^+W^\pm X$ is 0.95 pb [43,44].

The increase of the γp centre-of-mass energy by an order of magnitude with respect to fixed-target experiments [45] allows a search for generic heavy resonances, denoted by \mathcal{P} , with masses above 60 GeV in the reaction $\gamma p \rightarrow \mathcal{P} + X \rightarrow \text{jet} + \text{jet} + X$. While searches for such resonances formed by $q\bar{q}$ annihilation, such as Z' , have been performed [46] with similar sensitivity in this mass range, there are models such as Technicolour [47] which predict resonances⁵ produced preferentially by photon-gluon fusion. Such particles would not have been observed in earlier searches.

A search for the photoproduction of a new heavy resonance decaying into two jets has been performed in the mass range $60 < M_{\mathcal{P}} < 155$ GeV. The method described above has

⁴ Although the LO contribution to the production of W^\pm and Z^0 bosons is given by the resolved-photon processes (see Section 5), the resulting x_γ^{obs} distribution peaks at $x_\gamma^{\text{obs}} \sim 0.75$.

⁵ Some Technicolour models [48] predict the existence of light colour-octet, isospin-singlet pseudo-Goldstone bosons that would decay into two gluons.

also been used in this search to select the M^{jj} window for $|\cos\theta^*| < 0.6$. In this case, the background expected from QCD processes has been estimated by using the NLO QCD predictions with the normalisation obtained from a fit to the measured $d\sigma/dM^{\text{jj}}$ in the region of M^{jj} values well below that of the signal. Since there is no evidence for a signal, an upper limit on the cross section times the branching ratio into two jets for \mathcal{P} production, $\sigma_{e^+p \rightarrow e^+\mathcal{P}X} \cdot \text{Br}(\mathcal{P} \rightarrow \text{jet} + \text{jet})$, has been derived. The limit refers to the kinematic range defined by $Q^2 \leq 1 \text{ GeV}^2$, $134 < W < 277 \text{ GeV}$, $E_T^{\text{jet}} > 14 \text{ GeV}$, $-1 < \eta^{\text{jet}} < 2.5$ and $|\cos\theta^*| < 0.6$. The restriction to $|\cos\theta^*| < 0.6$ reduces the background from QCD-induced processes and the dependence on the spin and decay angular distribution of the heavy resonance (see Section 5). The upper limit on $\sigma_{e^+p \rightarrow e^+\mathcal{P}X} \cdot \text{Br}(\mathcal{P} \rightarrow \text{jet} + \text{jet})$ at 95% C.L. is shown in Fig. 5 as a function of $M_{\mathcal{P}}$.

10 Summary

Measurements of differential cross sections for dijet photoproduction have been made in e^+p collisions at a centre-of-mass energy of 300 GeV using 42.7 pb^{-1} of data collected with the ZEUS detector at HERA. The dijet cross sections refer to jets identified with the k_T cluster algorithm in the longitudinally invariant inclusive mode which were selected with $E_T^{\text{jet}} > 14 \text{ GeV}$ and $-1 < \eta^{\text{jet}} < 2.5$. The measurements were made in the kinematic region defined by $Q^2 \leq 1 \text{ GeV}^2$ and $134 < W < 277 \text{ GeV}$. The dijet differential cross section as a function of M^{jj} has been measured for $M^{\text{jj}} > 47 \text{ GeV}$ and $|\cos\theta^*| < 0.8$. Values of M^{jj} up to $\sim 160 \text{ GeV}$ are accessible with the present data. The NLO QCD calculations give a good description of the shape of the measured differential cross-section $d\sigma/dM^{\text{jj}}$.

The dijet cross section as a function of $\chi = (1 + |\cos\theta^*|)/(1 - |\cos\theta^*|)$ has been measured in several M^{jj} ranges. The dependence of the distribution $1/\sigma d\sigma/d\chi$ and of the ratio $R_\chi \equiv \frac{\sigma(1 < \chi < 4)}{\sigma(4 < \chi < 9)}$ on the dijet mass are found to be consistent with the predictions of NLO QCD in the M^{jj} range studied. The observed agreement in shape between data and the QCD calculations from $M^{\text{jj}} = 50 \text{ GeV}$ up to $M^{\text{jj}} = 139 \text{ GeV}$ confirms the validity of the pQCD description of photon-parton interactions down to distances of approximately $1.4 \cdot 10^{-3} \text{ fm}$.

The dijet events in the region $75 < M^{\text{jj}} < 100 \text{ GeV}$ have been used to derive an upper limit on the cross section for Z^0 production of $\sigma_{e^+p \rightarrow e^+Z^0X} < 5.9 \text{ pb}$ at 95% C.L. for $Q^2 \leq 1 \text{ GeV}^2$. Upper limits on the photoproduction of new heavy resonances decaying into two jets have been presented for $60 < M_{\mathcal{P}} < 155 \text{ GeV}$.

Acknowledgements

We thank the DESY Directorate for their strong support and encouragement. The re-

markable achievements of the HERA machine group were essential for the successful completion of this work and are greatly appreciated. We thank M. Klasen for valuable discussions and help in running his program for NLO QCD calculations.

References

- [1] C.H. Llewellyn Smith, *Phys. Lett. B* 79 (1978) 83;
I. Kang and C.H. Llewellyn Smith, *Nucl. Phys. B* 166 (1980) 413;
J.F. Owens, *Phys. Rev. D* 21 (1980) 54;
M. Fontannaz, A. Mantrach and D. Schiff, *Z. Phys. C* 6 (1980) 241.
- [2] W.J. Stirling and Z. Kunszt, *Proc. Workshop on Physics at HERA, Oct. 1987*, Volume 1, R. Peccei (ed.), DESY (1987), p. 331;
M. Drees and F. Halzen, *Phys. Rev. Lett.* 61 (1988) 275;
M. Drees and R.M. Godbole, *Phys. Rev. Lett.* 61 (1988) 682; *Phys. Rev. D* 39 (1989) 169;
H. Baer, J. Ohnemus and J.F. Owens, *Z. Phys. C* 42 (1989) 657; *Phys. Rev. D* 40 (1989) 2844.
- [3] UA2 Collaboration, P. Bagnaia et al., *Phys. Lett. B* 144 (1984) 283;
UA1 Collaboration, G. Arnison et al., *Phys. Lett. B* 158 (1985) 494;
UA1 Collaboration, C. Albajar et al., *Phys. Lett. B* 209 (1988) 127.
- [4] UA1 Collaboration, G. Arnison et al., *Phys. Lett. B* 177 (1986) 244.
- [5] CDF Collaboration, F. Abe et al., *Phys. Rev. Lett.* 62 (1989) 3020; *Phys. Rev. D* 41 (1990) 1722; *Phys. Rev. Lett.* 69 (1992) 2896; *Phys. Rev. D* 48 (1993) 998; *Phys. Rev. Lett.* 77 (1996) 5336; Erratum, *ibid.* 78 (1997) 4307;
CDF Collaboration, T. Affolder et al., *Phys. Rev. D* 61 (2000) 091101;
DØ Collaboration, B. Abbott et al., *Phys. Rev. Lett.* 80 (1998) 666; *Phys. Rev. Lett.* 82 (1999) 2457.
- [6] ZEUS Collaboration, M. Derrick et al., *Phys. Lett. B* 384 (1996) 401.
- [7] S. Catani et al., *Nucl. Phys. B* 406 (1993) 187.
- [8] M.H. Seymour, *Nucl. Phys. B* 513 (1998) 269.
- [9] M. Klasen, T. Kleinwort and G. Kramer, *Eur. Phys. J. direct C* 1 (1998) 1.
- [10] B.W. Harris and J.F. Owens, *Phys. Rev. D* 57 (1998) 5555.
- [11] S. Frixione and G. Ridolfi, *Nucl. Phys. B* 507 (1997) 315.

- [12] P. Aurenche et al., *Proc. Workshop on Future Physics at HERA, May 1996*, Volume 1, G. Ingelman, A. De Roeck and R. Klanner (eds.), DESY (1996), p. 570.
- [13] C.F. von Weizsäcker, *Z. Phys.* 88 (1934) 612;
E.J. Williams, *Phys. Rev.* 45 (1934) 729;
S. Frixione et al., *Phys. Lett. B* 319 (1993) 339.
- [14] B.W. Harris, M. Klasen and J. Vosseveld, *Proc. Workshop on Monte Carlo Generators for HERA Physics, Apr. 1998*, A.T. Doyle et al., (eds.), DESY (1999), p. 171.
- [15] ZEUS Collaboration, M. Derrick et al., *Phys. Lett. B* 293 (1992) 465.
- [16] ZEUS Collaboration, U. Holm (ed.), *The ZEUS Detector*, Status Report (unpublished), DESY, 1993, available on <http://www-zeus.desy.de/bluebook/bluebook.html>.
- [17] N. Harnew et al., *Nucl. Instr. and Meth. A* 279 (1989) 290;
B. Foster et al., *Nucl. Phys. B (Proc. Suppl.)* 32 (1993) 181;
B. Foster et al., *Nucl. Instr. and Meth. A* 338 (1994) 254.
- [18] M. Derrick et al., *Nucl. Instr. and Meth. A* 309 (1991) 77;
A. Andresen et al., *Nucl. Instr. and Meth. A* 309 (1991) 101;
A. Caldwell et al., *Nucl. Instr. and Meth. A* 321 (1992) 356;
A. Bernstein et al., *Nucl. Instr. and Meth. A* 336 (1993) 23.
- [19] J. Andruszków et al., DESY Report 92-066 (1992);
ZEUS Collaboration, M. Derrick et al., *Z. Phys. C* 63 (1994) 391;
ZEUS Luminosity Group, J. Andruszków et al., DESY Report 01-041 (2001).
- [20] ZEUS Collaboration, J. Breitweg et al., *Eur. Phys. J. C* 2 (1998) 61.
- [21] ZEUS Collaboration, J. Breitweg et al., *Eur. Phys. J. C* 4 (1998) 591.
- [22] H. Abramowicz, A. Caldwell and R. Sinkus, *Nucl. Instr. and Meth. A* 365 (1995) 508.
- [23] ZEUS Collaboration, M. Derrick et al., *Phys. Lett. B* 322 (1994) 287.
- [24] S.D. Ellis and D.E. Soper, *Phys. Rev. D* 48 (1993) 3160.
- [25] J. Huth et al., *Proc. of the 1990 DPF Summer Study on High Energy Physics*, E.L. Berger (ed.), Snowmass, Colorado, World Scientific (1992), p. 134.
- [26] H.-U. Bengtsson and T. Sjöstrand, *Comp. Phys. Comm.* 46 (1987) 43;
T. Sjöstrand, *Comp. Phys. Comm.* 82 (1994) 74.

- [27] G. Marchesini et al., *Comp. Phys. Comm.* 67 (1992) 465.
- [28] M. Glück, E. Reya and A. Vogt, *Phys. Rev. D* 46 (1992) 1973.
- [29] A.D. Martin, W.J. Stirling and R.G. Roberts, *Phys. Rev. D* 50 (1994) 6734.
- [30] H. Abramowicz, K. Charchuła and A. Levy, *Phys. Lett. B* 269 (1991) 458.
- [31] B. Andersson et al., *Phys. Rep.* 97 (1983) 31.
- [32] T. Sjöstrand, *Comp. Phys. Comm.* 39 (1986) 347;
T. Sjöstrand and M. Bengtsson, *Comp. Phys. Comm.* 43 (1987) 367.
- [33] B.R. Webber, *Nucl. Phys. B* 238 (1984) 492.
- [34] R. Brun et al., GEANT3, Technical Report CERN-DD/EE/84-1, CERN (1987).
- [35] C. Glasman, Ph.D. Thesis, Weizmann Institute of Science (1995), DESY-F35D-95-02; K. Desch, Ph.D. Thesis, Physikalisches Institut der Universität Bonn (1995), BONN-IR-95-13; Y. Yamazaki, Ph.D. Thesis, Institute for Nuclear Study, University of Tokyo (1996), INS-J-184.
- [36] ZEUS Collaboration, S. Chekanov et al., *Eur. Phys. J. C* 21 (2001) 443.
- [37] F. Jacquet and A. Blondel, *Proc. Study for an ep Facility for Europe*, U. Amaldi et al. (eds.), DESY 79/48 (1979), p. 377.
- [38] G. D'Agostini and D. Monaldi, *Z. Phys. C* 48 (1990) 467;
R. van Woudenberg et al., *Proc. Workshop on Physics at HERA, Oct. 1991*, Volume 2, W. Buchmüller and G. Ingelman (eds.), DESY (1992), p. 739.
- [39] ZEUS Collaboration, M. Derrick et al., *Phys. Lett. B* 348 (1995) 665.
- [40] H.L. Lai et al., *Phys. Rev. D* 55 (1997) 1280.
- [41] P. Aurenche, J.P. Guillet and M. Fontannaz, *Z. Phys. C* 64 (1994) 621.
- [42] B.L. Combridge and C.J. Maxwell, *Nucl. Phys. B* 239 (1984) 429.
- [43] U. Baur, J.A.M. Vermaseren and D. Zeppenfeld, *Nucl. Phys. B* 375 (1992) 3.
- [44] ZEUS Collaboration, J. Breitweg et al., *Phys. Lett. B* 471 (2000) 411.
- [45] E683 Collaboration, D. Alton et al., *Phys. Rev. D* 56 (1997) 5301.
- [46] UA2 Collaboration, J. Alitti et al., *Z. Phys. C* 49 (1991) 17; *Nucl. Phys. B* 400 (1993) 3.

- [47] S. Weinberg, Phys. Rev. D 19 (1979) 1277;
L. Susskind, Phys. Rev. D 20 (1979) 2619.
- [48] A. Bueno and F. Cornet, Phys. Lett. B 281 (1992) 369.

ZEUS

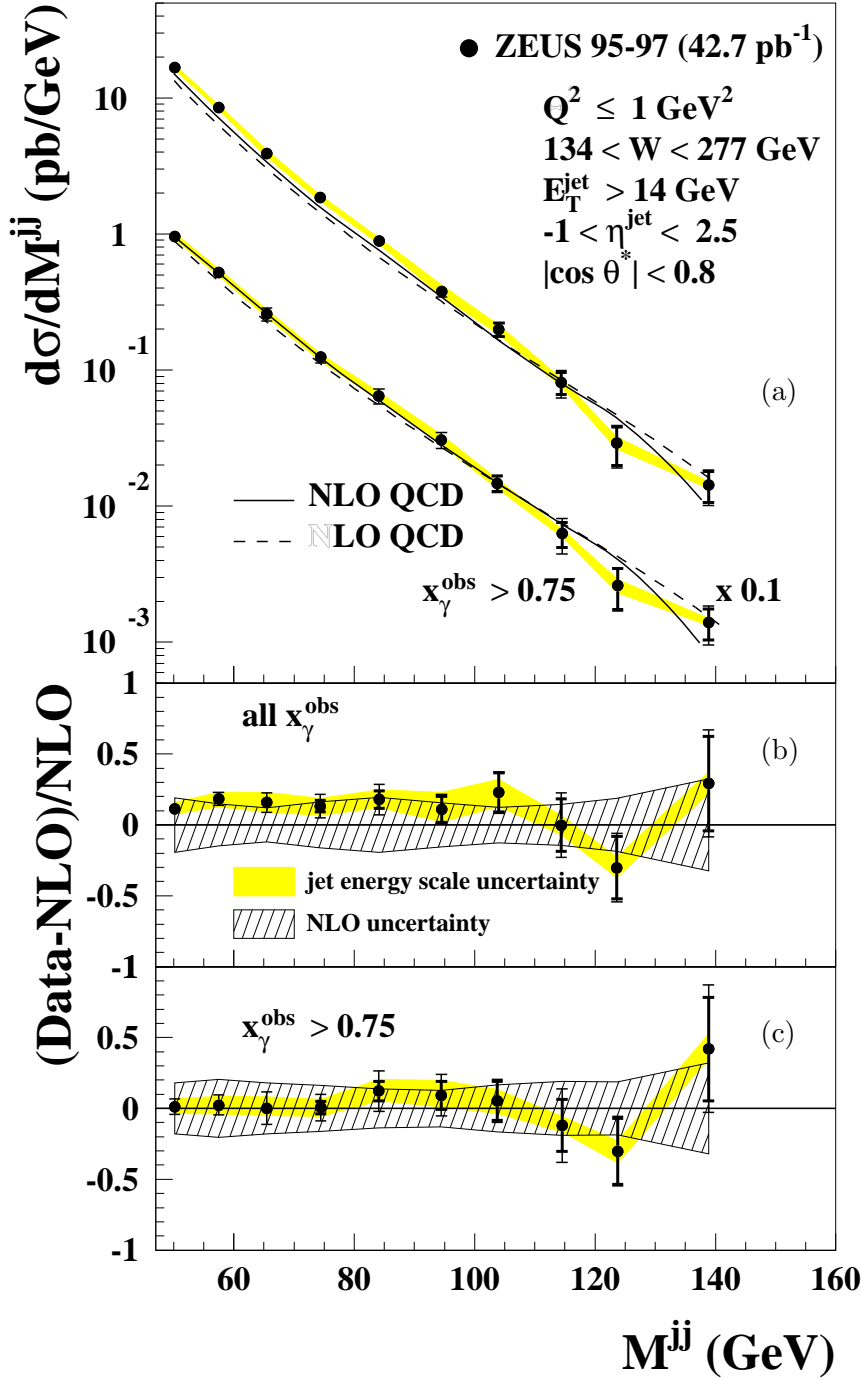


Figure 1: (a) Dijet cross-section $d\sigma/dM^{\text{jj}}$; the upper data points are for the full region in x_γ^{obs} and the lower points are for the region $x_\gamma^{\text{obs}} > 0.75$. The thick vertical bars represent the statistical uncertainties of the data, and the thin bars show the statistical and systematic uncertainties added in quadrature, except for that associated with the uncertainty in the absolute energy scale of the jets (shaded band). The LO (dashed line) and NLO (solid line) QCD parton-level calculations are shown. Both the measurements and calculations of $d\sigma/dM^{\text{jj}}$, for $x_\gamma^{\text{obs}} > 0.75$, have been multiplied by 0.1 for clarity of display; (b) the fractional difference between the measured $d\sigma/dM^{\text{jj}}$ and the NLO QCD calculation integrated over the full region in x_γ^{obs} ; (c) as (b), but for the region $x_\gamma^{\text{obs}} > 0.75$. In (b) and (c), the hatched bands display the uncertainty of the NLO QCD calculations.

ZEUS

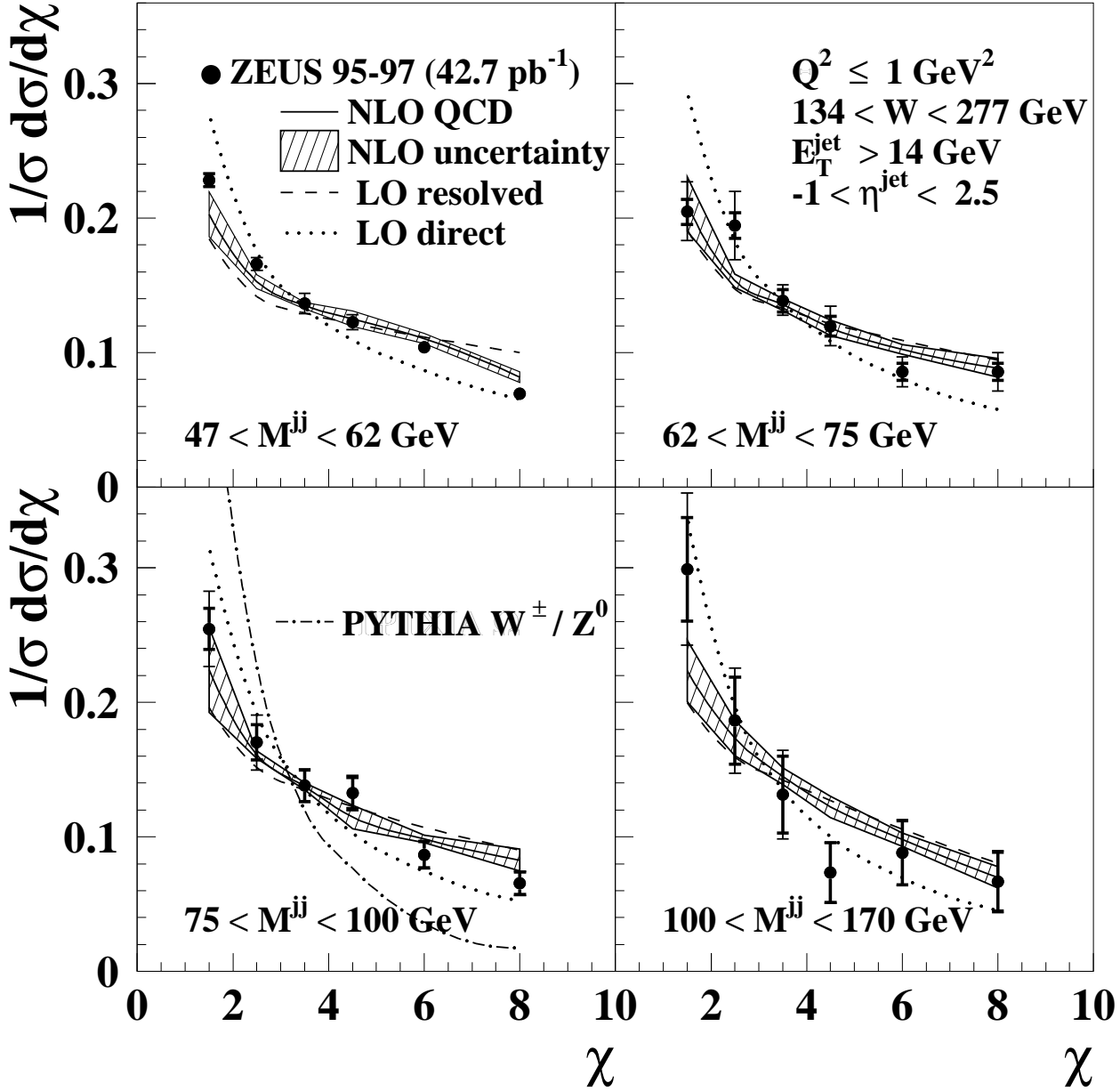


Figure 2: The normalised dijet cross sections, $1/\sigma d\sigma/d\chi$, in the full region of x_γ^{obs} , for four ranges in M^{jj} . The thick vertical bars represent the statistical uncertainties of the data while the thin bars show the statistical and systematic uncertainties added in quadrature. For comparison, NLO QCD parton-level calculations are shown as solid lines. The hatched bands display the uncertainty of the NLO QCD calculations. The LO QCD parton-level calculations for resolved (dashed lines) and direct (dotted lines) processes are also shown. The prediction of PYTHIA for the production of W^\pm and Z^0 bosons (dot-dashed line) is also shown in the region $75 < M^{\text{jj}} < 100 \text{ GeV}$.

ZEUS

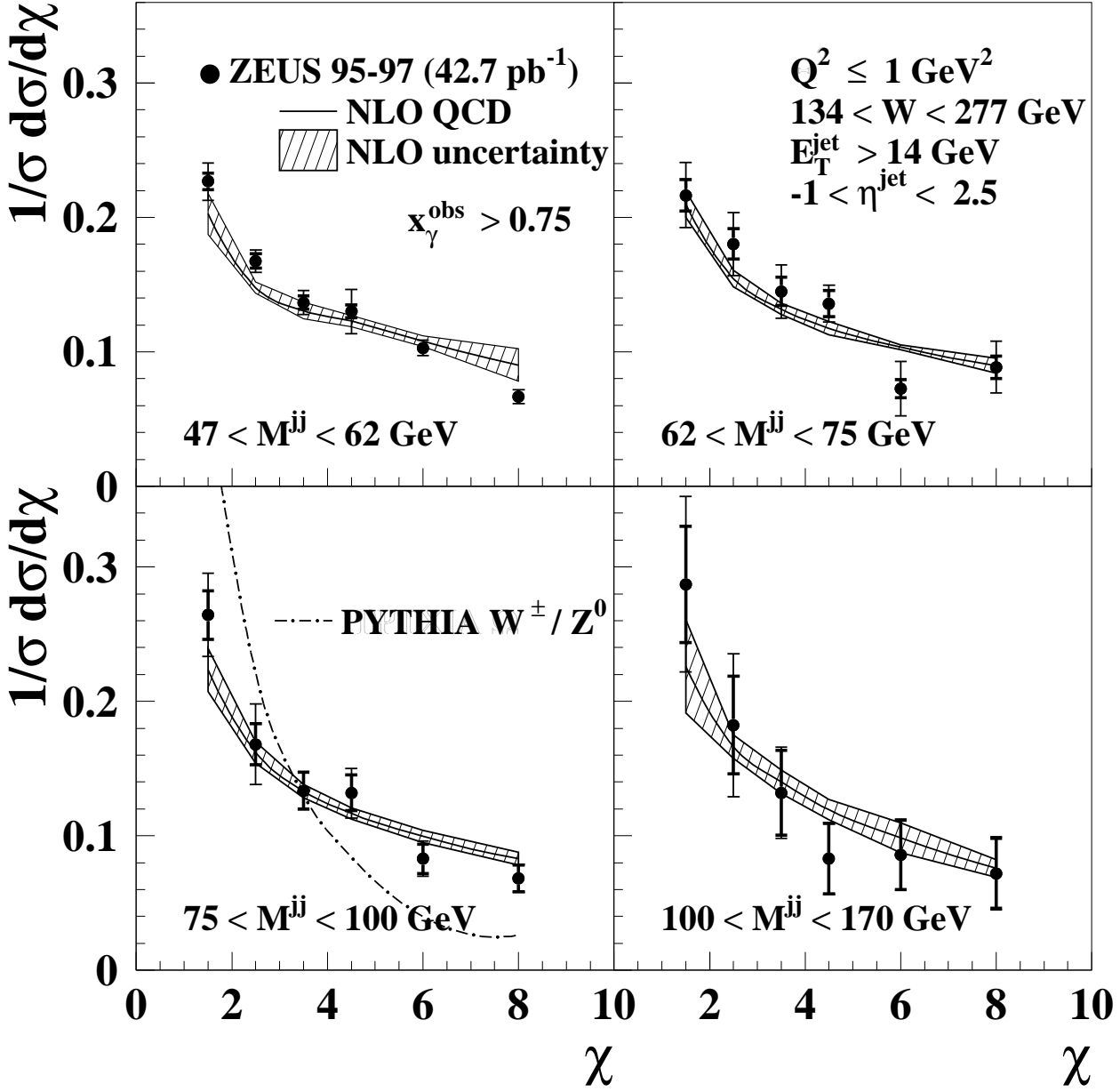


Figure 3: The normalised dijet cross sections $1/\sigma d\sigma/d\chi$, restricted to $x_\gamma^{\text{obs}} > 0.75$, for four ranges in M^{jj} . Other details are as described in the caption to Fig. 2.

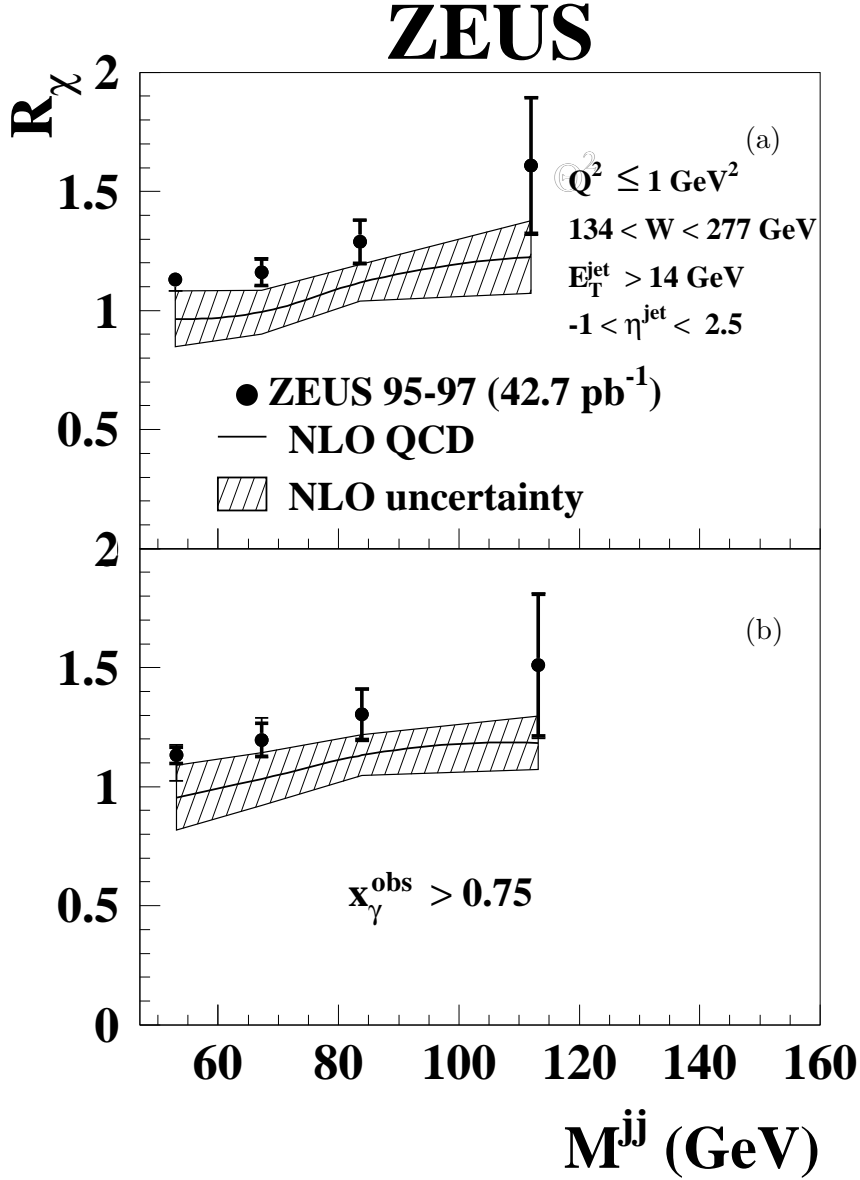


Figure 4: The cross-section ratio, $R_\chi = \frac{\sigma(1 < \chi < 4)}{\sigma(4 < \chi < 9)}$, as a function of M^{jj} : (a) integrated over the full region in x_γ^{obs} ; (b) for the region $x_\gamma^{\text{obs}} > 0.75$. The thick vertical bars represent the statistical uncertainties of the data while the thin bars show the statistical and systematic uncertainties added in quadrature. For comparison, the parton-level prediction of NLO QCD is shown as the solid line; the hatched band displays its uncertainty.

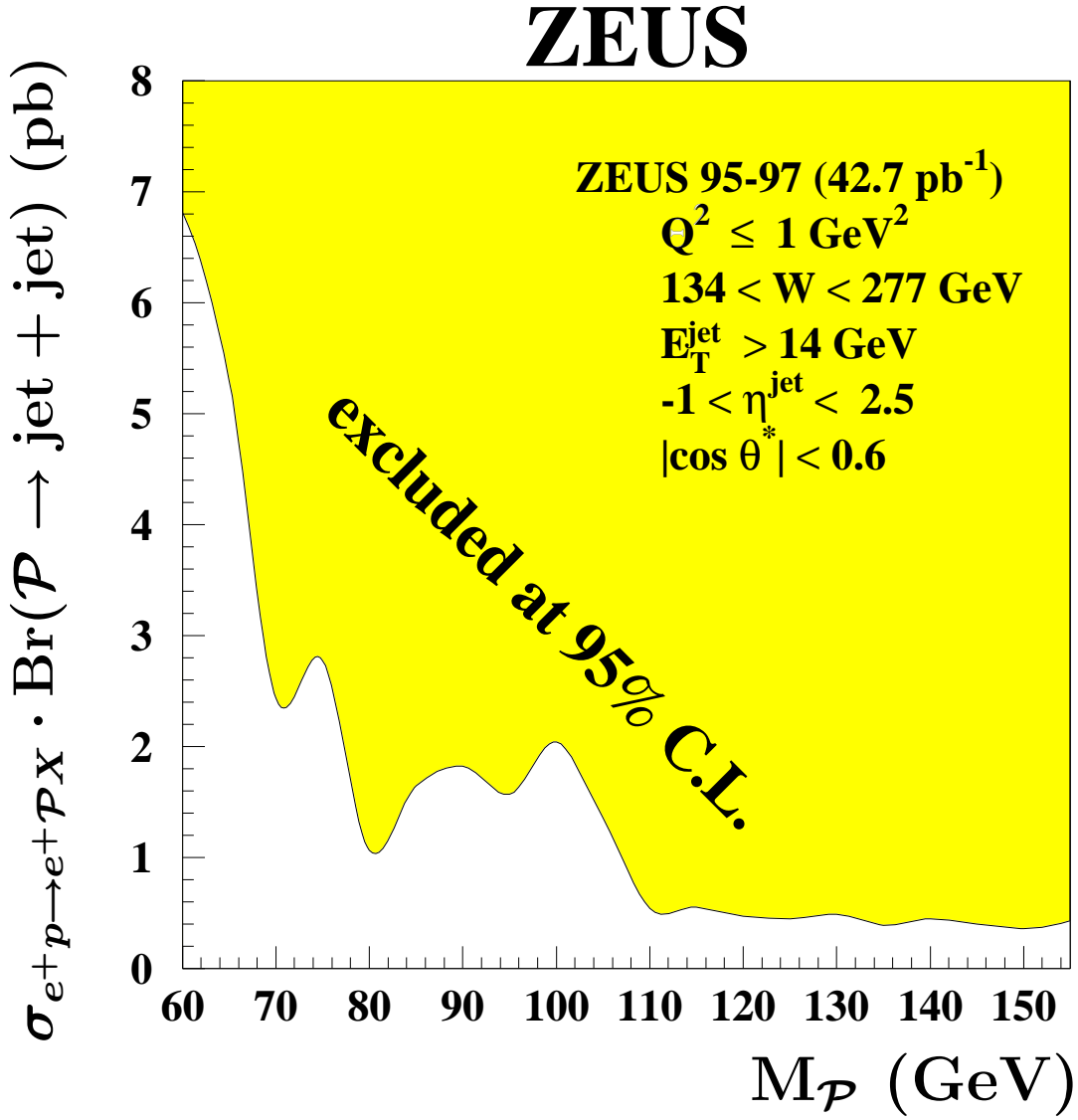


Figure 5: Upper limit at 95% C.L. on the cross section times branching ratio for the production of new heavy resonances decaying into two jets, $\sigma_{e+p \rightarrow e+P_X} \cdot \text{Br}(\mathcal{P} \rightarrow \text{jet} + \text{jet})$, as a function of the resonance mass, $M_{\mathcal{P}}$.